

PAPER • OPEN ACCESS

On cold atmospheric-pressure plasma jet induced DNA damage in cells

To cite this article: Nishtha Gaur *et al* 2021 *J. Phys. D: Appl. Phys.* **54** 035203

View the [article online](#) for updates and enhancements.

You may also like





- [Revisiting Tractable Strategies to Determine the Activity/Inactivity of Electrocatalysts towards \$O_2/OH\$ Production](#)
D. A. García-Osorio, Jorge Vazquez-Arenas and Raciél Jaimes
- [Human coronavirus inactivation by atmospheric pressure helium plasma](#)
Shota Sasaki, Shion Osana, Takahiro Kubota et al.
- [Investigation of the ORR Using the Double-Trap Intrinsic Kinetic Model](#)
M. Moore, A. Putz and M. Secanell



ECS
The
Electrochemical
Society
Advancing solid state &
electrochemical science & technology

DISCOVER
how sustainability
intersects with
electrochemistry & solid
state science research

On cold atmospheric-pressure plasma jet induced DNA damage in cells

Nishtha Gaur^{1,2,3,4,5} , Hirofumi Kurita⁶ , Jun-Seok Oh⁷ , Saki Miyachika⁶, Masafumi Ito⁷, Akira Mizuno⁶, Allison J Cowin¹, Sarah Allinson⁴, Robert D Short^{1,3,5} and Endre J Szili¹ 

¹ Future Industries Institute, University of South Australia, Adelaide, Australia

² Wound Management Innovation Cooperative Research Centre, Adelaide, Australia

³ Department of Chemistry, Lancaster University, Lancaster, United Kingdom

⁴ Department of Biomedical and Life Sciences, Lancaster University, Lancaster, United Kingdom

⁵ Materials Science Institute, Lancaster University, Lancaster, United Kingdom

⁶ Department of Applied Chemistry and Life Sciences, Toyohashi University of Technology, Toyohashi, Japan

⁷ Department of Electrical and Electronic Engineering, Meijo University, Nagoya, Japan

E-mail: nishtha.gaur@lancaster.ac.uk, endre.szili@unisa.edu.au and r.d.short1@lancaster.ac.uk

Received 1 June 2020, revised 26 August 2020

Accepted for publication 15 September 2020

Published 22 October 2020



CrossMark

Abstract

To investigate the potential role of the hydroxyl radical ($\bullet\text{OH}$) in cold atmospheric plasma (CAP) jet treatment, two fluorescence-based methodologies are utilised to measure DNA strand breaks. The first comprises a model system of a double-stranded DNA oligomer, where the respective strand ends are tagged with fluorophore and quencher molecules; and the second, a cell culture system reporting DNA strand breaks using the $\gamma\text{-H2AX}$ assay. During the various CAP jet treatments, optical emission spectroscopy is used to detect the $\bullet\text{OH}$ in the gas phase and electron spin resonance is used to detect the $\bullet\text{OH}$ in solution. The CAP jet production of the $\bullet\text{OH}$ is shown to correlate to CAP jet induced DNA damage both with the DNA model and in biological cells. Results indicate that the CAP jet induces a higher degree of DNA damage when the CAP plume is in contact with the target solution. The potential of a 'plasma screen' based upon a hydrogel film, as a method to remove the DNA-damaging $\bullet\text{OH}$ species from reaching skin cells, is shown to significantly reduce DNA damage whilst facilitating the delivery of hydrogen peroxide. These findings could aid in the development of CAP jet-based applications where DNA damage is the objective (e.g. in cancer treatment) and others where it is to be avoided, e.g. in open-wound treatment and dermatology.

Supplementary material for this article is available [online](#)

Keywords: reactive oxygen species (ROS), plasma jet, DNA damage, hydroxyl radicals (OH), plasma medicine, $\gamma\text{-H2AX}$, HaCaTs

(Some figures may appear in colour only in the online journal)

⁸ Current address: Graduate School of Engineering, Osaka City University, Sugimoto, Sumiyoshi, Osaka 558-8585, Japan

1. Introduction

II Potential healthcare applications for cold atmospheric plasma (CAP) include dermatology [1, 2], wound decontamination and healing [3, 4], cancer therapy [5] and dentistry [6]. The possible (beneficial) effects of CAP in healthcare are often attributed to the broad range of reactive oxygen and



Original content from this work may be used under the terms of the [Creative Commons Attribution 4.0 licence](#). Any further distribution of this work must maintain attribution to the author(s) and the title of the work, journal citation and DOI.

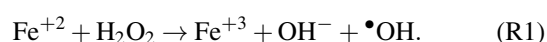
nitrogen species (RONS) that are delivered from plasma to and/or created within the biological target [7, 8]. In addition to RONS, physical components of CAP (electric field, UV photons, charged particles, radiation, etc.) also play a major role in plasma-induced biological effects in tissues [9–12].

Within the human body, endogenous RONS act as key cell-signalling molecules with the ability to control/intervene in a variety of cellular and physiological processes. For instance, through very specific and highly regulated mechanisms, hydrogen peroxide (H_2O_2) has been shown to induce cell proliferation, cell differentiation and angiogenesis (generally at concentrations of $<10 \mu\text{M}$), whilst inducing apoptosis, necrosis and growth arrest in cells at concentrations higher than 0.1 mM [13–15].

Similarly, the superoxide radical ($\text{O}_2^{\bullet-}$) and the hydroxyl radical ($\bullet\text{OH}$), along with H_2O_2 are produced by neutrophils and macrophages during the process of phagocytosis [16]. These act as potent microbiocidal agents that kill specific bacteria and viruses [17, 18]. Peroxynitrite (ONOO^-) and nitric oxide (NO) have been reported as important intercellular messenger molecules for cell signalling and neural network activation at low concentrations (nM range) [19].

Amongst the wide range of endogenous RONS, the $\bullet\text{OH}$ is regarded as an important species due to its highly reactive nature and the ability to directly react with almost all biomolecules including DNA, unlike H_2O_2 [20–22]. The $\bullet\text{OH}$ reacts with DNA either by abstracting hydrogen from the amine group in the DNA bases or from the carbon groups of the sugar moiety [22, 23]. The former will result in oxidative base damage, while the latter causes cleavage of the phosphodiester backbone, i.e. strand breaks.

In biological systems, H_2O_2 can form the $\bullet\text{OH}$ upon reaction with metal ions bound to the DNA (for example: copper ions present in chromosomes) [24] or present within the cells in normal conditions (such as ferric ions) [25] via Fenton chemistry (reaction 1).

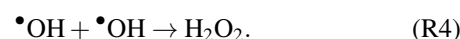
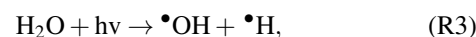
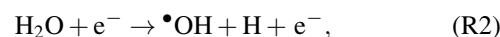


This intracellular production of the $\bullet\text{OH}$ is tightly regulated by anti-oxidant defense mechanisms which includes scavenging enzymes such as catalase, superoxide dismutase, glutathione peroxidase, peroxiredoxin and thioredoxin peroxidase [26, 27]. Another limiting/regulating factor for the production of the $\bullet\text{OH}$ in cells is the availability and location of metal ions, which are sequestered within the protein and DNA [28].

In certain healthcare applications, such as in the eradication of invading microbes or in cancer treatment, it is often desirable to induce detrimental changes in the target cells, such as irreversible DNA damage, in order to arrest the progression of a disease. However, in other applications such as the treatment of an open wound, the imperative should be to minimise unnecessary DNA damage.

If the objective is to produce the $\bullet\text{OH}$ within a biological target, the anti-oxidant defense mechanisms can be overcome through the exogenous production and delivery of RONS, e.g. through CAP treatment. During CAP treatment, the $\bullet\text{OH}$ is produced in the gas-phase (reaction 2) [29] and/or via

interaction between the UV photons and liquid surface through the process of UV photolysis (reaction 3) [30]. The $\bullet\text{OH}$ can be subsequently converted to stable H_2O_2 (reaction 4) through recombination with neighbouring molecules [30], which play an essential role in cellular signalling processes [31].



However generated, the plasma produced $\bullet\text{OH}$ has been linked to a number of biological effects including phagocytosis, apoptosis and DNA damage [32, 33]. This indicates that the plasma delivery of the highly reactive $\bullet\text{OH}$ can potentially be harnessed for the treatment of various refractory indications such as cancers. Given the potential beneficial effects of the $\bullet\text{OH}$ in plasma healthcare, yet at the same time considering its potential mutagenic risk, it is necessary to understand how to safely and effectively deliver the $\bullet\text{OH}$ to achieve specific biological effects.

To a certain degree, different biological effects can be achieved in plasma treatments by ‘tuning’ the plasma composition, including RONS, which can be accomplished by tailoring the design of the CAP device, or the CAP operational parameters (e.g. input power, frequency, flow rate) or in the manner of the CAP treatment (e.g. treatment distance, treatment time). Herein, we have investigated how the proximity of a target solution to a helium plasma jet influences the intrinsic plasma properties, how this correlates with the generation of the $\bullet\text{OH}$ in solution and the effects in terms of subsequent DNA modification, in the form of DNA strand breaks.

In an attempt to establish a ‘safer’ more real-world, implementable plasma treatment, where for example it is difficult to precisely control the plasma-target distance, the concept of a plasma screen (a hydrogel dressing) has been developed and is tested. By placing the hydrogel dressing in-between the biological target and CAP jet, we show that the delivery of the highly reactive $\bullet\text{OH}$ to the cells/tissue fluid is limited, without compromising the delivery of H_2O_2 . Such an approach may be beneficial for chronic wound treatments by preventing undesirable damage from the CAP to the surrounding healthy cells and tissue. The results and conclusions drawn from this study strengthen our knowledge about the interactions of CAP with biological targets (cells and DNA) and this knowledge may help in the future development of CAP technology in various biomedical applications.

2. Materials and methods

2.1. Helium CAP jet

The CAP jet assembly consisted of a glass tube with a 6 mm outer and 4 mm inner diameter, respectively. The glass tube

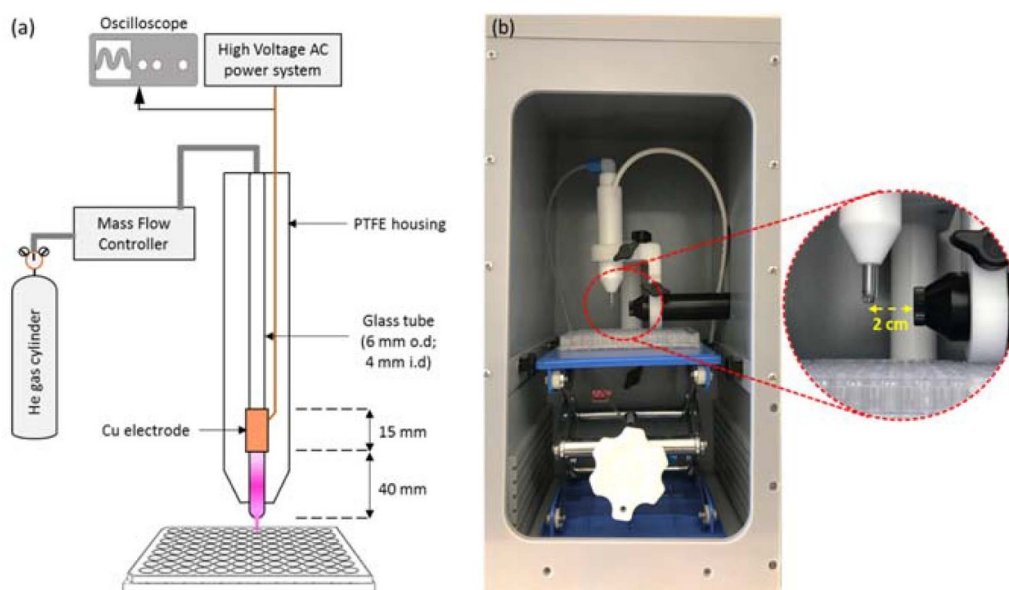


Figure 1. (a) A schematic of the CAP jet assembly. (b) A photograph of the CAP jet showing the position of the optical emission spectrometer optical fibre used to capture the optical emission *in situ* in a custom-built dark enclosure.

was tapered to $800\ \mu\text{m}$ at the nozzle. A single, cylindrical copper electrode of 15 mm in length and a distance of 40 mm from the nozzle, was fitted over the glass tube so that there was no visible air-gap between the glass and copper. The electrode was powered by a PVM500 (Information Unlimited, USA) power supply. The flow rate of high purity helium gas (BOC) through the glass tube was controlled by a digital mass flow controller (APEX, USA) and fixed at 1 standard litres per minute (slpm). The input voltage supplied to the electrode was fixed at $10\ \text{kV}_{\text{p-p}}$ (peak-to-peak) at a frequency of 30 kHz. A schematic of the plasma jet assembly is shown in figure 1(a).

2.2. Electrical and optical plasma diagnostics

The voltage and current during plasma operation were recorded with a commercial voltage probe (Tektronix P6015) and current monitor (Pearson Electronics, model 2877), respectively, connected to a digital oscilloscope (Tektronix TDS2014B). Optical emission between 300 and 750 nm, was measured with a commercial fibre-optic spectrometer (Ocean Optics, Model—Flame-TX-R1-ES, Grating—#31-500/250) through a collimating lens. Measurements were taken in a custom-built ‘dark box’ to prevent interference from ambient light, as shown in figure 1(b). The optical spectrometer was placed perpendicular with the direction of CAP jet. The emission from the plasma plume was measured laterally at a distance of 20 mm from the end of the nozzle of the glass tube of the CAP jet assembly. The integration time of the spectrometer was set to 10 ms with a wavelength range of 280–780 nm.

2.3. Plasma screen

A 4 mm thick commercially available hydrogel dressing, IntraSite Conformable (Smith & Nephew, Catalogue no. 66000324), was used in this study. IntraSite Conformable

is a hydrogel cream on a non-woven dressing material. The dressing was cut into approximately $20 \times 20\ \text{mm}^2$ pieces. For the plasma treatments through hydrogel dressing, $400\ \mu\text{l}$ of the cell culture media or a model DNA (see section 2.4 below) in a 96-well plate was treated with the CAP jet. The hydrogel dressing was slightly pressed down into the well to ensure it contacted the solution.

2.4. Preparation of 4-(2-hydroxyethyl)-1-piperazineethanesulfonic acid (HEPES) buffer

HEPES buffer was prepared by dissolving 238.3 mg of HEPES (Sigma-Aldrich, Catalogue no. 3375), 624 mg of sodium chloride (Optigen Scientific, Catalogue no. OS-22760), 22.4 mg of sodium hydroxide (Sigma-Aldrich, Catalogue no. 367176) and 29.22 mg of Ethylenedinitrilo tetraacetic acid disodium salt (Optigen Scientific, Catalogue no. OS-53170) in 100 ml of water (Sigma-Aldrich, Catalogue no. 95283). The pH of the HEPES solution was adjusted to 7.4 using 10 mM of NaOH solution. The solution was filtered using a $0.2\ \mu\text{m}$ syringe filter.

2.5. Assessment of DNA strand breaks in HEPES buffer

Double-stranded DNA with a length of 12 nucleotides was purchased from Sigma-Aldrich. The forward oligomer was labelled with a fluorescein amidite (6-FAM) fluorophore at the 5' end with sequence: 5'-[6-FAM]GCACTGAAGCGC-3'. The reverse oligomer was labelled with Black Hole Quencher (BHQ-1) at the 3' end with complementary sequence: 5'-GCGCTTCAGTGC[BHQ-1]-3'. Intact, the BHQ-1 inhibits the fluorescence of 6-FAM in the double-stranded DNA. DNA strand break(s) leads to a separation of the BHQ-1 and 6-FAM and a switch-on of fluorescence, as shown in figure 2.

A volume of $405\ \mu\text{l}$ and $753\ \mu\text{l}$ of 10 mM Tris-base buffer was added to 40.5 nmol of forward and 75.3 nmol of reverse

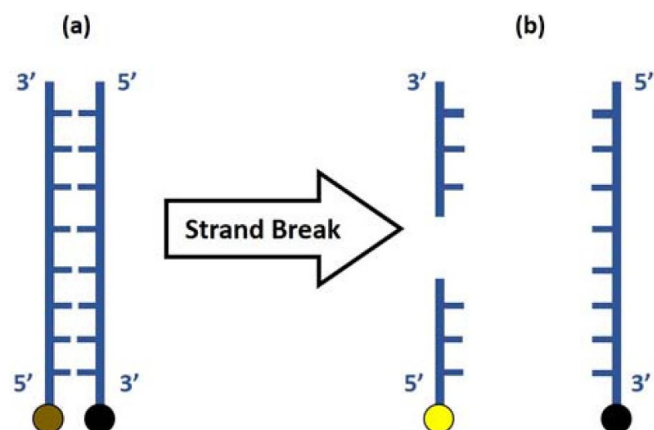


Figure 2. Schematic of the double-strand DNA used as a fluorescent probe to assess DNA strand breaks. (a) The DNA molecule consists of a fluorophore (6-FAM, brown dot) at the 5' end of one strand and a quencher (BHQ-1, black dot) at the 3' end of the second strand. (b) One (as shown) or multiple DNA strand breaks anywhere on the molecule result in a separation of the fluorophore and quencher and subsequent switch-on of fluorophore fluorescence (yellow dot).

oligomer, respectively, to obtain oligomer solutions of 100 μM each. Synthetic DNA solution with a working concentration of 1 μM was prepared by diluting both combined oligomer solutions in HEPES buffer. The double-stranded DNA probe was prepared by heating this solution at 95 $^{\circ}\text{C}$ for 3 min to first reversibly denature the double-stranded DNA, followed by annealing at ambient temperature for 3 h in the dark to allow re-hybridisation. This procedure ensured the correct conformation of the double-stranded DNA in solution.

A volume of 200 μl of the DNA-HEPES solution was then dispensed into the well of a 96-well plate. The direct CAP jet treatment of the DNA solution (without a hydrogel dressing on top) was performed at two different distances of 5 mm and 10 mm such that the plasma plume is in contact (at $d = 5$ mm) and not in contact ($d = 10$ mm) with the DNA solution (figure 3(a) and (b)). For the indirect CAP jet treatment, 400 μl of DNA solution in a 96-well plate was treated through the screen (hydrogel dressing) at $d = 1$ mm (figure 3(c)). Fluorescence measurements were recorded using a microplate reader (BMG Labtech Fluostar Optima) at an excitation wavelength of 498 nm and emission wavelength of 522 nm.

2.6. Measurement of H_2O_2

The concentration of H_2O_2 in HEPES after the CAP jet treatment was measured using an electrochemical probe (ISO-HPO-2, World Precision Instruments) interfaced to the Free Radical analyser (TBR4100-416, World Precision Instruments) [34].

2.7. Measurement of the $\bullet\text{OH}$

Electron spin resonance (ESR) spectroscopy was used to measure the $\bullet\text{OH}$ delivered by the CAP jet into solution. 5-(2,2-Dimethyl-1,3-propoxy cyclophosphoryl)-5-methyl-1-pyrroline N-oxide (CYPMPO) was used as the spin-trapping

agent [35]. A 100 μl volume of 10 mM CYPMPO (Shidai system, Catalogue no. RR-121-A) was prepared in HEPES and treated with the plasma jet in a 96-well plate. Following CAP jet treatment, the ESR reaction sample was transferred to a flat cell (JEOL resonance, Catalogue no. DP-1055). The ESR signal was measured using an ESR spectrometer (JES-X310, JEOL Resonance, Tokyo, Japan), operating at 9.42 GHz and at 100 kHz field modulation. The settings of the spectrometer were: centre magnetic field = 335.6 mT; field width = ± 15.0 mT; microwave power = 4 mW; modulation amplitude = 0.1 mT; and time constant = 0.1 s. The relative intensities of the ESR spectra were calculated by referencing against a manganese (Mn^{2+}) internal standard. Relative magnetic intensities were plotted by subtracting peak signal intensities of untreated (control) from the intensities of CAP jet treated solution.

2.8. HaCaT cell culture

HaCaT keratinocyte-like cells were cultured in DMEM (Gibco[®], Catalogue no. 11965118) supplemented with 10% (v/v) fetal bovine serum (Gibco[®], Catalogue no. 1099141), 100 IU ml^{-1} of penicillin and 100 $\mu\text{g ml}^{-1}$ of streptomycin (Gibco[®], Catalogue no. 15140122) in T75 cell culture flasks (Corning[®], Catalogue no. 353110). The cells were cultured at 37 $^{\circ}\text{C}$ in a humidified incubator with 5% CO_2 . The cells were passaged following the trypsinisation process such that a total of 7000 cells in 200 μl of DMEM was added to wells of a 96-well tissue cell culture plate for the direct CAP jet treatment (without screen on top). For the CAP jet treatments through the screen, 400 μl cell suspension (with 7000 cells in total) was treated for 240 s at $d = 1$ mm. The hydrogel dressing was not removed from the plate until the $\gamma\text{-H2AX}$ assay was performed. After the CAP jet treatments, the cells (with and without the hydrogel dressing) were incubated overnight at 37 $^{\circ}\text{C}$, 5% CO_2 , prior to the $\gamma\text{-H2AX}$ assay.

2.9. $\gamma\text{-H2AX}$ assay for the assessment of DNA strand breaks in HaCaTs

The cells were fixed with 4% (v/v) paraformaldehyde solution (ProSciTech, Catalogue no. EMS15710-S), permeabilised with 0.5% (v/v) Triton X-100 (Sigma-Aldrich, Catalogue no. T8787) and blocked with 3% (w/v) bovine serum albumin (BSA) solution (Sigma-Aldrich, Catalogue no. A7906). The cells were incubated with the primary antibody mouse monoclonal [9F3] to $\gamma\text{-H2AX}$ [phospho S139] (Abcam, Catalogue no. ab26350) diluted at 1:1000 and the secondary antibody goat anti-mouse IgG H&L [Alexa Fluor[®] 488] (Abcam, Catalogue no. ab150113) diluted at 1:1000. The nucleus was stained using 300 nM of 4',6-diamidino-2-phenylindole (DAPI, Thermo Fischer, Catalogue no. D1306).

Fluorescence images were recorded on an Olympus microscope using a DP80 camera. The images were taken at an excitation/emission of 358/461 nm for DAPI and 495/519 nm for Alexa Fluor[®]. The exposure time for all of the images was kept constant at 137.93 ms for the DAPI channel and 500 ms for

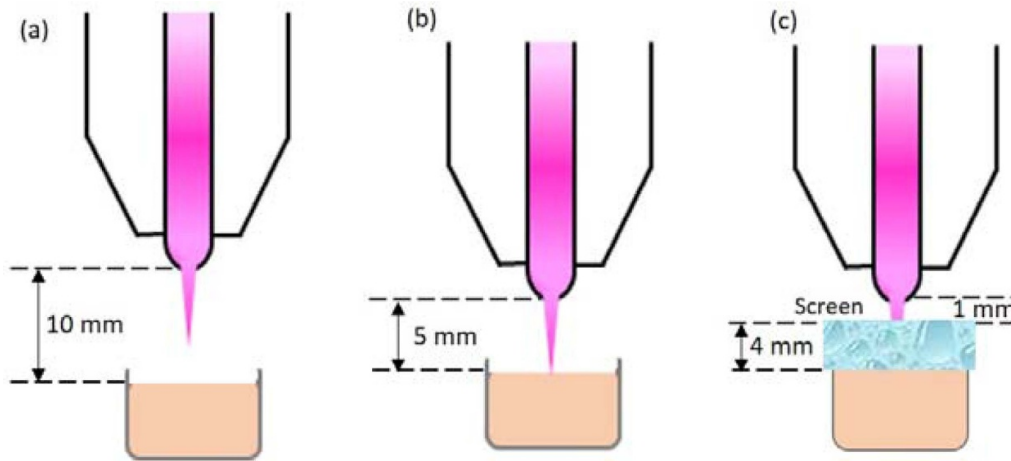


Figure 3. Experimental setup for the three types of CAP jet treatment conditions: (a) non-contact (plasma plume is not in contact with the target solution in a well of a 96-well plate); (b) contact (plasma plume is in contact with the target solution); and (c) through a ca. 4 mm screen (a hydrogel dressing is placed on top of the well such that the plasma plume is not in direct contact with the target solution).

the Alexa Fluor® channel. The γ -H2AX positive nuclei from a total of up to 100 cells (DAPI stained nuclei) were counted for each condition for three biologically independent replicates. The images were processed using the Olympus cellSens Dimension software.

3. Results

The voltage waveform and input power (P_{in}) of the CAP jet for each treatment parameter (shown in figures 4(a)–(c)) was measured by electrical diagnosis. A discharge current (I_d) was calculated by subtracting the displacement current (I_{dis}) from the total current (I_t) as per the equation below [36]:

$$I_d = I_t - I_{dis}, \quad (1)$$

where I_{dis} is the current measured in absence of the plasma discharge (i.e. without applying V_{p-p}) and I_t is current measured for the plasma discharge with the applied V_{p-p} . Values of V and I_d were used to calculate averaged P_{in} at a fixed frequency (f) using the formula:

$$P_{in} = f \int_0^t V(t) \times I_d(t) dt. \quad (2)$$

Figure 4(a) shows that the sinusoidal waveforms of V_{p-p} for the He plasma discharges are identical for the direct (plasma contact and non-contact with a HEPES buffer solution) CAP jet treatments and for treatment through the screen (plasma contacts the hydrogel dressing). However, as shown in figure 4(b), the shape and peak value of I_d varies according to the target. The highest I_d (2.21 mA), with a narrow peak width, is seen when the CAP jet is in contact with the liquid, the lowest is seen for the non-contact mode (0.63 mA), and the peak value for I_d is somewhere between these two when the CAP jet is in contact with the screen (1.46 mA). A similar trend is observed for P_{in} as shown in figure 4(c). The closer treatment

distance produced the highest value of P_{in} at 9.26 W. However, CAP jet treatment through the screen resulted in a P_{in} value of 4.89 W, double than that of the non-contact treatment condition, but half for the solution contact condition. Considering the current pulse width, the averaged-power for the contact treatment condition and the through-screen treatment is not very different (1.64 ± 0.03 for contact and 1.25 ± 0.04 for screen, respectively).

Following the electrical characterisation, an optical diagnosis of the CAP jet was performed by optical emission spectroscopy (OES). The typical optical emission spectra from 280 to 780 nm are shown in figure 4(d). For all treatment conditions (contact, non-contact and through the screen), the spectra in figure 4(d) confirm the presence of N_2 species (N_2^+ second positive and N_2^* first negative systems) by spectral lines in the UV-A region (310–430 nm), excited He at 471.3, 501.6, 587.6, 667.8, and 706.5 nm and excited O at 777.5 nm (assignments made from the NIST Atomic Spectra Database). A slight increase in the signal intensities for He* is observed at the closer distance between the CAP jet and target of 5 mm (compared to the 10 mm treatment distance). No $\bullet OH$ emission is observed in the plasma plume for the non-contact treatment condition. However, when plasma is touching the liquid surface (contact condition) or the screen, $\bullet OH$ emission is observed at 308 nm. The peak intensity for $\bullet OH$ is higher for plasma treatment through the screen than the direct contact treatment. The $\bullet OH$ emission spectra normalised to the He peak at 706.5 nm is shown in figure 5 to directly compare the differences in $\bullet OH$ emission, which corroborates with our discussion directly above.

The extent of DNA damage induced by the CAP jet by the direct CAP jet and screen treatments was assessed using the double-strand DNA fluorescent probe synthetic DNA probe. Direct CAP jet treatments for the non-contact and contact condition were conducted at 1 slpm for 15, 30 and 60 s. A third condition comprises treatment through the screen for 240 s (to produce a solution H_2O_2 concentration in the same range as

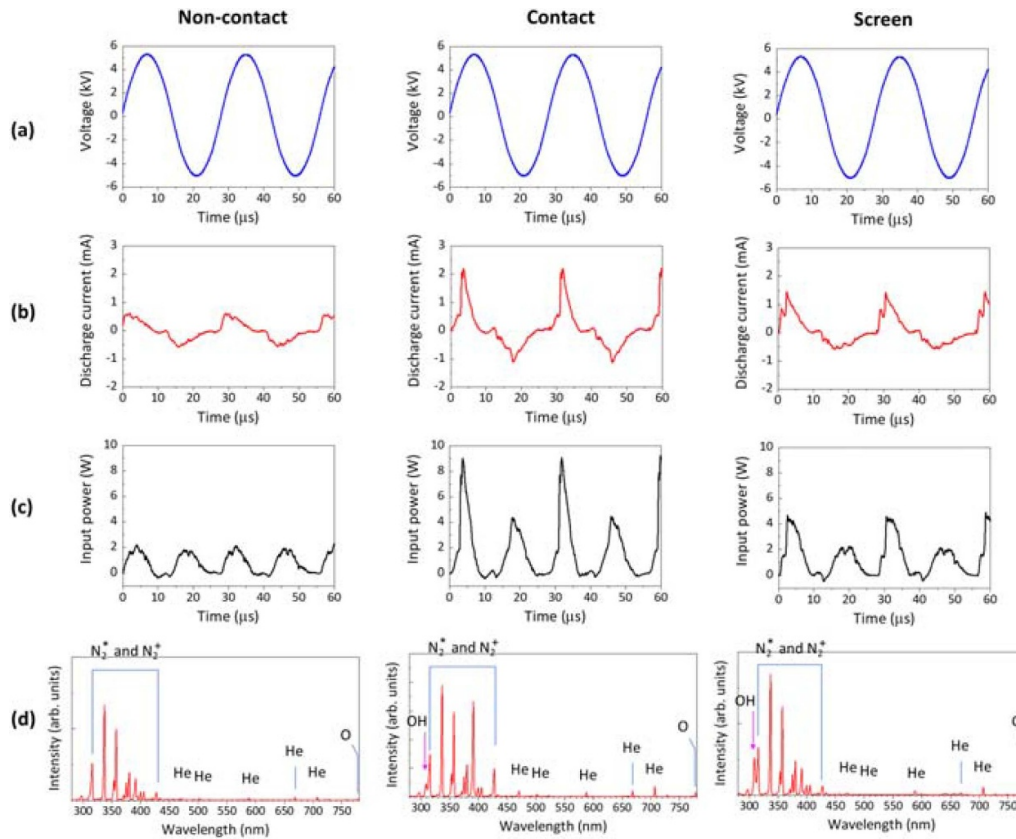


Figure 4. The electrical and optical emission properties of the CAP jet during treatment of the HEPES buffer solution. The four rows show (a) V_{p-p} , (b) I_d , (c) P_{in} and (d) optical emission spectra between 280 and 780 nm. The three columns show results taken for each of the three CAP jet treatment conditions—i.e. plasma plume non-contact with HEPES buffer solution, plasma plume contact with HEPES buffer solution and through screen treatment (with the plasma plume in contact with the hydrogel dressing).

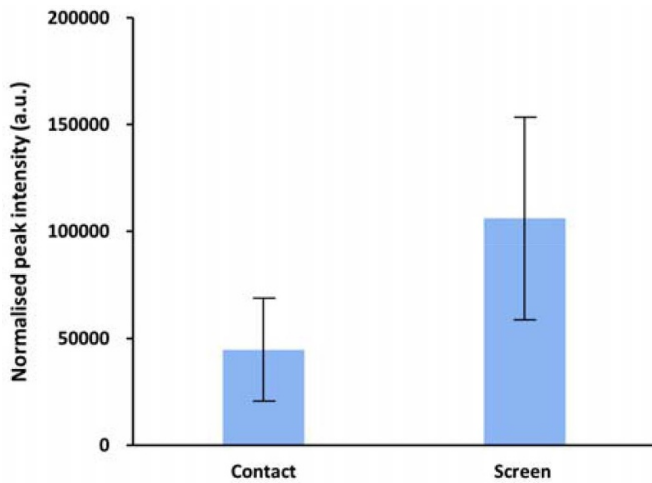


Figure 5. Normalised $\bullet OH$ peak intensities for the direct (contact) and indirect (through screen) plasma treatment conditions. The $\bullet OH$ emission intensities at 308 nm are normalised against the He emissions at 706.52 nm.

contact treatments; this will be discussed later) with the plasma plume in contact with the screen.

To measure the relative amount of DNA breaks, the normalised fluorescence intensity (FI) of the synthetic DNA probe was measured by:

$$\text{Normalised FI} = \left(\frac{\text{FI of plasma treated probe}}{\text{FI of untreated probe}} \right) - 1. \quad (3)$$

The data are presented in figure 6 and represent the mean value of three replicates ($n = 3$) and \pm standard deviation (STDEV) error of the mean. For both contact and non-contact conditions, the results in figure 6 show that the extent of DNA damage increases with the plasma exposure time. At any equivalent exposure time, a much higher degree of DNA damage is observed for the contact *versus* non-contact scenario. These data allow the assessment that in tissue fluid, 60 s of ‘non-contact’ CAP jet treatment induces an equivalent level of DNA damage to 15 s of ‘contact’ CAP jet treatment. Since DNA damage was not eliminated with any of the direct CAP jet treatments, these data provide the basis to assess the role of the screen to limit DNA damage. As shown in figure 6, exposing synthetic DNA to plasma for 240 s through the screen reduces DNA damage to a lower level than the 15 s of direct CAP jet treatments in both contact and non-contact conditions. This implies that by employing the screen between the target and the CAP jet, the extent of DNA damage can be significantly restricted.

As previously stated, it is speculated that the $\bullet OH$ delivered by the CAP jet is a major contributing factor in DNA damage, and that a reduction in DNA damage can be achieved by inhibiting the delivery of the $\bullet OH$ to the target (for example to

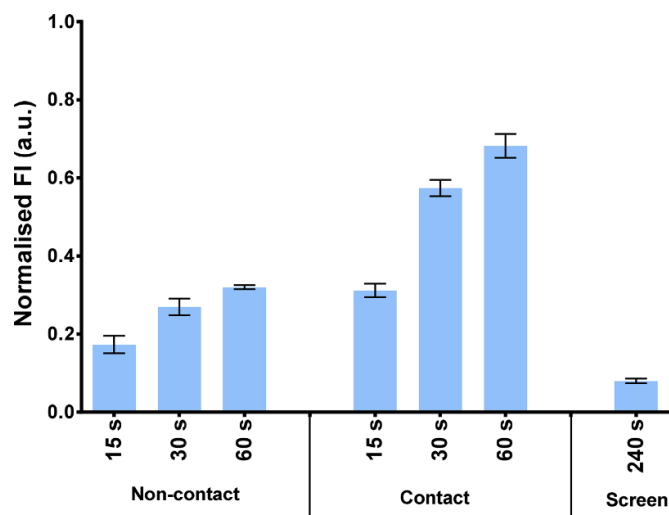


Figure 6. DNA damage measured in terms of DNA strand breaks shown by normalised FI. Direct CAP jet treatments were carried out at 1 slpm for 15, 30 and 60 s or through the screen for 240 s. The data above represents the mean value of three replicates ($n = 3$) and \pm standard deviation (STDEV) error of the mean.

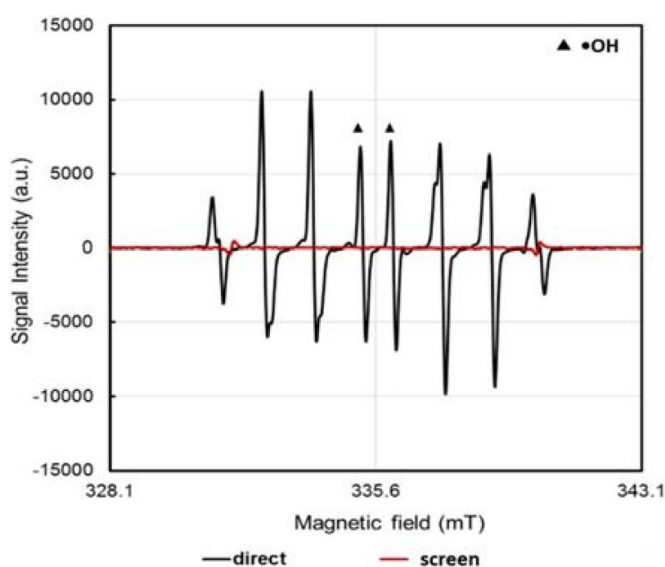


Figure 7. The ESR spectrum of the CYPMPO-OH adduct in HEPES after it was directly treated with the CAP jet ($d = 10$ mm, treatment time = 60 s) and indirectly through the hydrogel dressing/screen ($d = 1$ mm, treatment time = 240 s).

cells). Therefore, we assessed by ESR the relative amount of the \bullet OH delivered by the non-contact and contact direct CAP jet treatments and the screen treatment into the HEPES buffer. A typical ESR spectrum is shown in figure 7 for a direct CAP jet treatment and screen treatment. As shown in figure 7, when CYPMPO spin-trap in HEPES was directly treated with the CAP jet, the signal for the CYPMPO-OH adduct (i.e. \bullet OH) is clearly observed. However, in the presence of the screen repeating the experiment, there are now no visible peaks corresponding to the trapped \bullet OH. This suggests that the plasma screen can inhibit the CAP jet generation of the \bullet OH in the

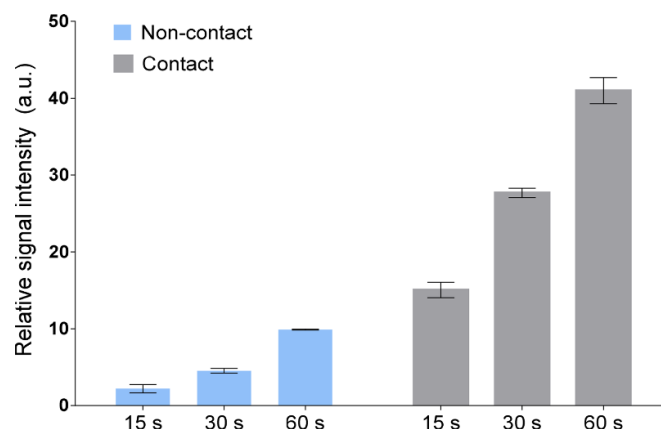


Figure 8. The relative signal intensities of the \bullet OH after direct CAP jet treatments of the CYPMPO spin-trap in HEPES buffer. The peak intensities were calculated by referencing to a Mn^{2+} internal standard. Data are expressed as the mean \pm STDEV ($n = 3$).

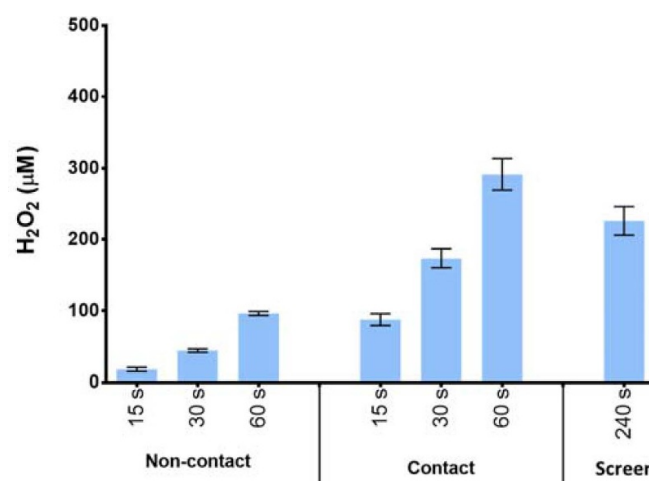


Figure 9. Concentration of H₂O₂ in HEPES generated by the direct CAP jet treatments and by the screen treatment.

HEPES, presumably by quenching the \bullet OH within the gel matrix.

The relative signal intensities for the \bullet OH in the ESR spectrum (calculated using the Mn^{2+} internal standard) for each CAP jet treatment parameter was calculated, and the results are shown in figure 8. As seen in figure 8, the relative signal intensities of the \bullet OH peak increases as function of the CAP jet treatment time, for both non-contact and contact conditions. However, the production of the \bullet OH is higher in the contact condition as compared to non-contact.

In the next set of experiments the concentration of H₂O₂ delivered by the CAP jet into HEPES in non-contact and contact conditions and in the presence of the screen were measured (figure 9). H₂O₂ was used to give an indication of the total RONS concentration on the basis that H₂O₂ is the major longer-lived RONS generated in aqueous solution for the He CAP jet configuration utilised in this study [37–39]. Moreover, H₂O₂ plays a significant role in cell proliferation and other important signalling mechanisms [31]. As shown in figure 9,

the concentrations of H_2O_2 increases in a dose-dependent manner. Higher concentrations of H_2O_2 are produced for the contact condition (up to 300 μM) than the non-contact (up to 100 μM). However, a shorter treatment time of 15 s in contact condition generates an equivalent concentration of H_2O_2 compared to the longer treatment time of 60 s in the non-contact condition. It is also evident that the CAP jet can deliver a similar concentration of H_2O_2 through the screen as compared to the direct CAP jet treatments.

The results so far show that the screen method of treatment can inhibit CAP jet induced DNA strand breaks for naked DNA freely suspended in HEPES. A further step in this study was to evaluate if this result could be translated to preventing DNA damage in skin cells. Therefore, in the following experiment, the γ -H2AX assay was performed using HaCaT keratinocytes that were subjected to the direct CAP jet treatment and to the screen treatment. The γ -H2AX assay is a marker for the DNA damage response (DDR), e.g. after a DNA strand break event in cells. To confirm that the biological effects are induced by CAP treatment, neutral He gas treatments (i.e. no plasma) were performed as a negative control (figure SI.03 (available online at stacks.iop.org/JPhysD/54/035203/mmedia) of the supplementary information). A neutral He gas treatment did not induce any DDR. Figure 10 shows a series of immunofluorescence images for all cell nuclei stained with DAPI-stained (blue) and γ -H2AX positive (green) nuclei captured 24 h after performing each of the treatments. The percentage of nuclei displaying phosphorylated H2AX (γ -H2AX) are calculated to provide a measure of the percentage of DNA strand breaks (figure 11). The percentage of DNA-strand breaks for each treatment condition is calculated using the following formula:

$$\text{Percentage of DNA strand breaks} = \frac{\text{Total number of gamma H2AX positive nuclei}}{\text{Total number of nuclei}} \times 100. \quad (4)$$

The results of the γ -H2AX assay in figures 10 and 11 show that all direct plasma jet treatments activate the DDR in HaCaT cells, as compared to the untreated (control) cells ($p < 0.05$). The DNA strand breaks manifest in γ -H2AX positive nuclei, as shown in figure 10. The number of γ -H2AX nuclei increase with the treatment time and are higher with the plasma plume in contact with the cell media during treatment. A marginal increase γ -H2AX nuclei is observed for the screen treatment ($p > 0.05$). Figure 10 also highlights different types of γ -H2AX staining—pan-nuclear pattern, wherein the entire nucleus shows green γ -H2AX stain (e.g. in case of 15 s direct contact CAP jet treatment) and focal pattern, wherein distinct γ -H2AX foci are formed in the nuclei (e.g. in case of screen treatment). The frequency of pan-nuclear stained cells increased with the treatment time for non-contact and contact direct CAP jet treatments.

CAP jet treatments can potentially change the pH and temperature of the cell media that (in addition to RONS such as the $\bullet\text{OH}$) might influence cellular activity. However, although we were unable to measure pH or temperature of the CAP jet

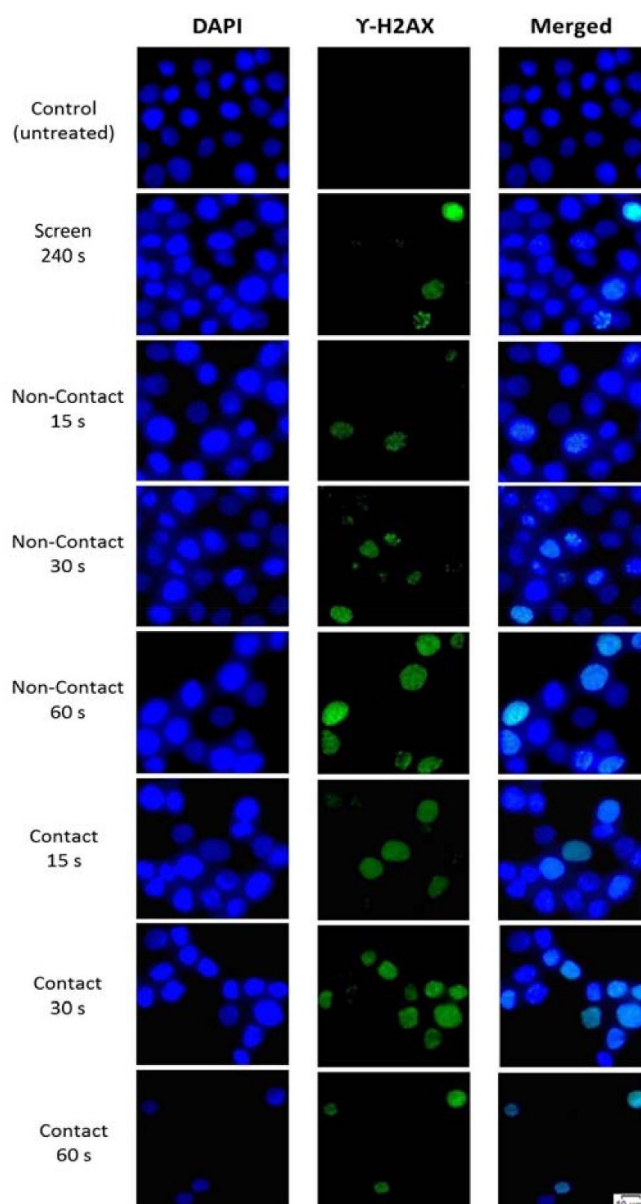


Figure 10. Micrographs from the γ -H2AX assay for direct CAP jet and screen treatments. The first, second and third column show the immunofluorescence images of DAPI stained nuclei, γ -H2AX positive nuclei and the overlayed images of columns 1 and 2, respectively.

treated media (because our pH and temperature probes were incompatible with the experimental set-up), based on our previous studies [40–42] and studies by other groups [43–45], we expect that neither pH nor temperature would have significantly impacted the cell results presented in this study.

4. Discussion

Previously, we have shown that H_2O_2 does not directly induce DNA strand breaks in a number modelled environments including surrogates of tissue fluid, cells and tissue [41]. This is in agreement with Verlacket *et al*, who also found that H_2O_2 does not directly break the phosphodiester backbone of DNA

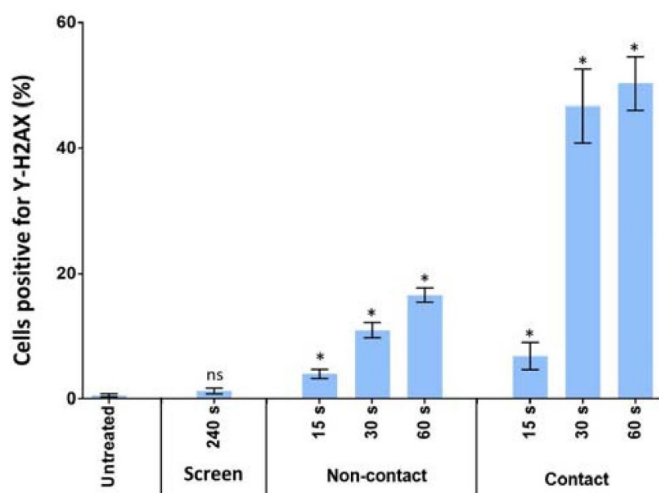


Figure 11. Percentage of DNA-strand breaks observed in HaCaT cells the γ -H2AX assay following direct CAP jet and screen treatments. Untreated control cells are shown for comparison. The γ -H2AX positive nuclei from a total of up to 100 cells (DAPI stained nuclei) were counted. Multi-way ANOVA was used to determine the statistical significance of the values. The values with * marks represent statistically significantly different values compared to the untreated ($p < 0.05$), whereas ns implies 'not-significant' ($p > 0.05$) i.e. the values are statistically insignificant compared to untreated.

through a simulation study [46]. With the premise that the longer-lived RONS delivered by the plasma into the target are not involved in direct DNA damage, we focused on the highly reactive $\bullet\text{OH}$, also recognised for its ability to directly induce DNA strand breaks in cells (e.g. in x-ray radiation therapy).

The emission spectra obtained from OES provides information of the presence of oxygen and nitrogen radicals (and metastables) in the plasma-phase (figure 4(d)). Although He^* , O^* and N_2 species were produced in all the CAP jet treatment conditions (contact, non-contact and screen), the emission peak for the $\bullet\text{OH}$ only became prominent when the plasma plume was in contact with the target (HEPES, cell media or screen). Furthermore, the signal intensity for the $\bullet\text{OH}$ increased as the treatment distance reduced from 5 mm (direct contact treatment) to 1 mm (through-screen treatment). At small distances, the plasma induces higher evaporation of water, thus creating a source of more water molecules that can be dissociated by UV photons, emanating from the CAP jet, into the $\bullet\text{OH}$. Secondary reactions with the highly reactive RONS (e.g. the $\bullet\text{OH}$) in the solution generate longer-lived but less reactive molecules such as H_2O_2 and NO_2^- [47, 48].

In the CAP jet treatment through the screen, the hydrogel dressing quenches the $\bullet\text{OH}$ within the hydrogel matrix (which was confirmed by the ESR results in figure 7). This prevented the delivery of the $\bullet\text{OH}$ into the target solutions. However, the screen facilitated the delivery of longer-lived H_2O_2 (figure 9). It should be noted that these findings are not limited to the 'commercial' dressing used in this study, but are also applicable to other types of hydrogels. We showed that a simple hydrogel film fabricated from gelatin (figure SI.02

of supplementary information) can significantly perturb the delivery of the $\bullet\text{OH}$ cf to the direct plasma jet treatments. The short-lived oxygen species, e.g. the $\bullet\text{OH}$ and O^* produced near the screen, can undergo reactions to form secondary RONS including H_2O_2 near and within the screen surface. These longer-lived species, along with other plasma species, may accumulate within the screen and undergo subsequent hydration or solvation before penetrating through the screen via a yet-to-be defined slow molecular transport process [38]. These reactions may lead to production of secondary RONS such as the $\text{O}_2^{\bullet-}$ and ONOO^- . In our study we also detected the production of $\text{O}_2^{\bullet-}$ in treatment through the screen (figure SI.01 in supplementary information). The low levels of DNA strand breaks observed in solution (figures 6 and 11), despite the presence of screen inhibiting the generation of the $\bullet\text{OH}$ in solution (figure 7), can be linked to the formation of the $\text{O}_2^{\bullet-}$ and potentially other species. Further indication that other CAP jet generated molecules might also be involved in DNA strand breaks is seen by a similar level of DNA strand breaks produced between the 60 s non-contact treatment and 15 s contact treatment (figure 6) despite the latter producing more of the $\bullet\text{OH}$ in solution (figure 8). Studying the potential role of other CAP jet generated molecules involved in DNA strand breaks could be the subject of an interesting follow-up study.

To assess the biological significance of this result, DNA damage was assessed in HaCaT keratinocyte cells. If cells experience DNA damage such as DNA strand breaks, cells will initiate the DDR to repair DNA [49]. The earliest DDR process, which occurs within seconds after DNA damage, is phosphorylation of the histone variant H2AX to form γ -H2AX, which is mediated by phosphatidylinositol 3-kinase related kinases (PIKK) [50]. γ -H2AX formation is important for recruiting the DNA repair factors, the proteins important for cell cycle progression and the repair and remodelling of chromatin and DNA [51]. Therefore, γ -H2AX is considered as a good marker for DNA damage [52, 53].

In this study, we utilised a commercially available hydrogel dressing as screen to shield the target solution from the CAP jet to prevent the delivery of the $\bullet\text{OH}$ (figure 7) that mitigated DNA damage in the HaCaT cells (figures 10 and 11). The differential staining showing the pan-nuclear pattern and focal pattern for γ -H2AX after the direct CAP jet and screen treatments (figure 10), indicates different types of cellular response to the DNA damage. Studies conducted with UV rays and ionising irradiation have observed similar staining patterns [53, 54]. The focal staining pattern can be linked to localised DDR, while the pan-nuclear staining pattern indicates apoptotic (or pre-apoptotic) cells. Therefore, it is fair to say that CAP jet-induced effects in cells are a complex phenomenon, and that the γ -H2AX assay can serve as a good biomarker to distinguish DDR cells from apoptotic cells. The results from figure 10 imply that at shorter CAP jet treatment distances and/or longer exposure durations where there is an enhanced production/delivery of H_2O_2 and $\bullet\text{OH}$, cells undergo apoptosis (pan-nuclear cells). However, during CAP jet treatment through the screen, where the delivery of the $\bullet\text{OH}$ to the cells is limited, localised DDR (focal staining) rather than

apoptosis is observed. Overall, these results indicate that the $\bullet\text{OH}$ generated by the CAP jet treatments has a major role in causing DNA damage.

5. Conclusion

In this study, we show that a hydrogel dressing can screen out the $\bullet\text{OH}$ from being generated in solution during CAP jet treatment. We show that preventing the delivery of the $\bullet\text{OH}$ during CAP jet treatment, completely abrogates the occurrence of DNA strand breaks and DNA damage in HaCaT cells, which is not possible with the direct CAP jet treatments in this study. However, the screen approach still enables the delivery of the CAP jet generated H_2O_2 (a well-known antimicrobial agent and cell stimulatory molecule) at a concentration in the same range as the direct CAP jet treatments investigated in this study. These data indicate that the screen is a promising development for minimising unwanted potential genotoxic events in cells such as for applications in CAP jet treatments of open wounds.

Acknowledgments

NG, EJS, AJC and RDS express gratitude to the Australian Government's Cooperative Research Centre's Program and the Wound Management Innovation CRC for partially supporting this research through project SP09-02. EJS acknowledges the support from the Australian Research Council through the Future Fellowship (No. FT190100263) award. HK acknowledges JSPS KAKENHI Grant Number (26390096, 17K05095) and the Naito Research Grant. AM acknowledges a MEXT KAKENHI Grant Number 24108005. JSO and MI acknowledge MEXT Supported Program for the Strategic Research Foundation at Private Universities (S1511021).

ORCID iDs

Nishtha Gaur  <https://orcid.org/0000-0003-2756-6963>
 Hirofumi Kurita  <https://orcid.org/0000-0002-2538-6590>
 Jun-Seok Oh  <https://orcid.org/0000-0003-3227-8544>
 Endre J Szili  <https://orcid.org/0000-0002-5165-1490>

References

- [1] Heinlin J, Isbary G, Stolz W, Morfill G, Landthaler M, Shimizu T, Steffes B, Nosenko T, Zimmermann J L and Karrer S 2011 Plasma applications in medicine with a special focus on dermatology *J. Eur. Acad. Dermatol. Venereol.* **25** 1–11
- [2] Xiong Z, Cao Y, Lu X and Du T 2011 Plasmas in tooth root canal *IEEE Trans. Plasma Sci.* **39** 2968
- [3] Isbary G et al 2012 Successful and safe use of 2 min cold atmospheric argon plasma in chronic wounds: results of a randomized controlled trial *Br. J. Dermatol.* **167** 404–10
- [4] Isbary G et al 2010 A first prospective randomized controlled trial to decrease bacterial load using cold atmospheric argon plasma on chronic wounds in patients *Br. J. Dermatol.* **163** 78–82
- [5] Keidar M, Walk R, Shashurin A, Srinivasan P, Sandler A, Dasgupta S, Ravi R, Guerrero-Preston R and Trink B 2011 Cold plasma selectivity and the possibility of a paradigm shift in cancer therapy *Br. J. Cancer* **105** 1295–301
- [6] Arora V et al 2014 Cold atmospheric plasma (CAP) in dentistry *Dentistry* **4** 1–6
- [7] Graves D B 2017 Mechanisms of plasma medicine: coupling plasma physics, biochemistry, and biology *IEEE Trans. Radiat. Plasma Med. Sci.* **1** 281–92
- [8] Graves D B and Bauer G 2018 Key roles of reactive oxygen and nitrogen species *Comprehensive Clinical Plasma Medicine: Cold Physical Plasma for Medical Application*, ed H-R Metelmann, T von Woedtke and K-D Weltmann (Cham: Springer) pp 71–82
- [9] Robert E, Darny T, Dozias S, Iseni S and Pouvesle J M 2015 New insights on the propagation of pulsed atmospheric plasma streams: from single jet to multi jet arrays *Phys. Plasmas* **22** 122007
- [10] Vandamme M et al 2012 ROS implication in a new antitumor strategy based on non-thermal plasma *Int. J. Cancer* **130** 2185–94
- [11] Szili E J, Bradley J W and Short R D 2014 A 'tissue model' to study the plasma delivery of reactive oxygen species *J. Phys. D: Appl. Phys.* **47** 152002
- [12] Collier G, Robert E, Lenoir A, Vandamme M, Darny T, Dozias S, Kieda C and Pouvesle J M 2014 Plasma jet-induced tissue oxygenation: potentialities for new therapeutic strategies *Plasma Sources Sci. Technol.* **23** 012005
- [13] Stone J R and Collins T 2002 The role of hydrogen peroxide in endothelial proliferative responses *Endothelium* **9** 231–8
- [14] Klyubin I V, Kirpichnikova K M and Gamaley I A 1996 Hydrogen peroxide-induced chemotaxis of mouse peritoneal neutrophils *Eur. J. Cell Biol.* **70** 347–51
- [15] Clément M V and Pervaiz S 2001 Intracellular superoxide and hydrogen peroxide concentrations: a critical balance that determines survival or death *Redox Rep.* **6** 211–4
- [16] Darr D and Fridovich I 1994 Free radicals in cutaneous biology *J. Invest. Dermatol.* **102** 671–5
- [17] Riley P 1994 Free radicals in biology: oxidative stress and the effects of ionizing radiation *Int. J. Radiat. Biol.* **65** 27–33
- [18] Wang L et al 2007 Hypochlorous acid as a potential wound care agent: part I. Stabilized hypochlorous acid: a component of the inorganic armamentarium of innate immunity *J. Burns Wounds* **6** e5
- [19] Liebmann J, Scherer J, Bibinov N, Rajasekaran P, Kovacs R, Gesche R, Awakowicz P and Kolb-Bachofen V 2011 Biological effects of nitric oxide generated by an atmospheric pressure gas-plasma on human skin cells *Nitric Oxide* **24** 8–16
- [20] Ma Y, Gong X, He B, Li X, Cao D, Li J, Xiong Q, Chen Q, Chen B H and Liu Q H 2018 On the quantification of the dissolved hydroxyl radicals in the plasma-liquid system using the molecular probe method *J. Phys. D: Appl. Phys.* **51** 155205
- [21] Halliwell B and Aruoma O I 1991 DNA damage by oxygen-derived species its mechanism and measurement in mammalian systems *FEBS Lett.* **281** 9–19
- [22] Dizdaroğlu M, Jaruga P, Birincioglu M and Rodriguez H 2002 Free radical-induced damage to DNA: mechanisms and measurement *Free Radic. Biol. Med.* **32** 1102–15
- [23] Valko M, Izakovic M, Mazur M, Rhodes C J and Telser J 2004 Role of oxygen radicals in DNA damage and cancer incidence *Mol. Cell. Biochem.* **266** 37–56
- [24] Prütz W A 1994 Interaction between glutathione and Cu(II) in the vicinity of nucleic acids *Biochem. J.* **302** 373–82
- [25] Prousek J 2007 Fenton chemistry in biology and medicine *Pure Appl. Chem.* **79** 2325–38
- [26] Andreyev A Y, Kushnareva Y E, Murphy A N and Starkov A A 2015 Mitochondrial ROS metabolism: 10 years later *Biochemistry (Mosc.)* **80** 517–31

- [27] Bindoli A and Rigobello M P 2013 Principles in redox signaling: from chemistry to functional significance *Antioxid. Redox Signal.* **18** 1557–93
- [28] Halliwell B, Clement M V and Long L H 2000 Hydrogen peroxide in the human body *FEBS Lett.* **486** 10–13
- [29] Bruggeman P and Schram D C 2010 On OH production in water containing atmospheric pressure plasmas *Plasma Sources Sci. Technol.* **19** 045025
- [30] Bruggeman P et al 2016 Plasma–liquid interactions: a review and roadmap *Plasma Sources Sci. Technol.* **25** 053002
- [31] Sies H 2017 Hydrogen peroxide as a central redox signaling molecule in physiological oxidative stress: oxidative eustress *Redox Biol.* **11** 613–9
- [32] Wiseman H and Halliwell B 1996 Damage to DNA by reactive oxygen and nitrogen species: role in inflammatory disease and progression to cancer *Biochem. J.* **313** 17–29
- [33] Halliwell B and Gutteridge J M C 1984 Oxygen toxicity, oxygen radicals, transition metals and diseases *Biochem. J.* **219** 1–14
- [34] Taniguchi N and Gutteridge J 2000 *Experimental Protocols for Reactive Oxygen and Nitrogen Species* (Oxford: Oxford University Press)
- [35] Kurita H et al 2020 Strand breaks and chemical modification of intracellular DNA induced by cold atmospheric pressure plasma irradiation *PloS One* **15** e0232724
- [36] Szili E J et al 2018 Modelling the helium plasma jet delivery of reactive species into a 3D cancer tumour *Plasma Sources Sci. Technol.* **27** 014001
- [37] Oh J-S, Szili E J, Gaur N, Hong S-H, Furuta H, Kurita H, Mizuno A, Hatta A and Short R D 2016 How to assess the plasma delivery of RONS into tissue fluid and tissue *J. Phys. D: Appl. Phys.* **49** 304005
- [38] Oh J-S, Szili E J, Ito S, Hong S-H, Gaur N, Furuta H, Short R D and Hatta A 2015 Slow molecular transport of plasma-generated reactive oxygen and nitrogen species and O₂ through Agarose as a surrogate for tissue *Plasma Med.* **5** 125–43
- [39] Oh J-S, Szili E J, Gaur N, Hong S-H, Furuta H, Short R D and Hatta A 2015 *In-situ* UV absorption spectroscopy for monitoring transport of plasma reactive species through Agarose as surrogate for tissue *J. Photopolym. Sci. Technol.* **28** 439–44
- [40] Hong S-H, Szili E J, Fenech M, Gaur N and Short R D 2017 Genotoxicity and cytotoxicity of the plasma jet-treated medium on lymphoblastoid WIL2-NS cell line using the cytokinesis block micronucleus cytome assay *Sci. Rep.* **7** 3854
- [41] Szili E J et al 2017 The assessment of cold atmospheric plasma treatment of DNA in synthetic models of tissue fluid, tissue and cells *J. Phys. D: Appl. Phys.* **50** 274001
- [42] Oh J-S et al 2016 How plasma induced oxidation, oxygenation, and de-oxygenation influences viability of skin cells *Appl. Phys. Lett.* **109** 203701
- [43] Nicol M J et al 2020 Antibacterial effects of low-temperature plasma generated by atmospheric-pressure plasma jet are mediated by reactive oxygen species *Sci. Rep.* **10** 3066
- [44] Mohades S, Barekzi N and Laroussi M 2014 Efficacy of low temperature plasma against SCABER cancer cells *Plasma Process. Polym.* **11** 1150–5
- [45] Volotskova O, Hawley T S, Stepp M A and Keidar M 2012 Targeting the cancer cell cycle by cold atmospheric plasma *Sci. Rep.* **2** 636
- [46] Verlackt C C W, Neyts E C, Jacob T, Fantauzzi D, Golkaram M, Shin Y-K, van Duin A C T and Bogaerts A 2015 Atomic-scale insight into the interactions between hydroxyl radicals and DNA in solution using the ReaxFF reactive force field *New J. Phys.* **17** 103005
- [47] Eva Stoffels Y S and Graves D B 2008 Cold atmospheric plasma: charged species and their interactions with cells and tissues *IEEE Trans. Plasma Sci.* **36** 1441–57
- [48] Lu X, Naidis G V, Laroussi M, Reuter S, Graves D B and Ostrikov K 2016 Reactive species in non-equilibrium atmospheric-pressure plasmas: generation, transport, and biological effects *Phys. Rep.* **630** 1–84
- [49] Jackson S P and Bartek J 2009 The DNA-damage response in human biology and disease *Nature* **461** 1071–8
- [50] Burma S, Chen B P, Murphy M, Kurimasa A and Chen D J 2001 ATM phosphorylates histone H2AX in response to DNA double-strand breaks *J. Biol. Chem.* **276** 42462–7
- [51] Mariotti L G, Pirovano G, Savage K I, Ghita M, Ottolenghi A, Prise K M and Schettino G 2013 Use of the γ -H2AX assay to investigate DNA repair dynamics following multiple radiation exposures *PloS One* **8** e79541
- [52] Bonner W M, Redon C E, Dickey J S, Nakamura A J, Sedelnikova O A, Solier S and Pommier Y 2008 GammaH2AX and cancer *Nat. Rev. Cancer* **8** 957–67
- [53] de Feraudy S, Revet I, Bezrookove V, Feeney L and Cleaver J E 2010 A minority of foci or pan-nuclear apoptotic staining of gammaH2AX in the S phase after UV damage contain DNA double-strand breaks *Proc. Natl Acad. Sci. USA* **107** 6870–5
- [54] Ding D, Zhang Y, Wang J, Zhang X, Gao Y, Yin L, Li Q, Li J and Chen H 2016 Induction and inhibition of the pan-nuclear gamma-H2AX response in resting human peripheral blood lymphocytes after X-ray irradiation *Cell Death Discov.* **2** 16011